Radiation-Induced Damage and Recovery of Ultra Nano-Crystalline Diamond: Towards Applications in Harsh Environments

Aiden A. Martin,[*,†] Jorge Filevich,[‡] Marcus Straw,[‡] Steven Randolph,[‡] Aurélien Botman,[‡] Igor Aharonovich,[¶] and Milos Toth[¶]

†*Physical and Life Sciences Directorate, Lawrence Livermore National Laboratory, Livermore, California 94550, USA*

‡*Thermo Fisher Scientific (formerly FEI Company), 5350 Northeast Dawson Creek Drive, Hillsboro, Oregon 97214-5793, USA*

¶*School of Physics and Advanced Materials, University of Technology, Sydney, 15 Broadway, Ultimo, New South Wales 2007, Australia*

E-mail: martin248@llnl.gov

Abstract

Ultra nano-crystalline diamond (UNCD) is increasingly being used in the fabrication of devices and coatings due to its excellent tribological properties, corrosion resistance and bio-compatibility. Here, we study its response to irradiation with kilo-electronvolt electrons as a controlled model for extreme ionizing environments. Real time Raman spectroscopy reveals that the radiation damage mechanism entails dehydrogenation of UNCD grain boundaries, and we show that the damage can be recovered by annealing at 883 K. Our results have significant practical implications for the implementation of UNCD in extreme environment applications, and indicate that the films can be used as radiation sensors.

KEYWORDS: electron beam induced damage, ultra nano-crystalline diamond, Raman spectroscopy, reaction kinetics, dehydrogenation, grain boundaries, damage recovery

Introduction

Ultra nano-crystalline diamond (UNCD) is a nanostructured film consisting of 2 - 5 nm diamond grains within a matrix of 0.4 - 0.6 nm wide sp^3/sp^2 grain boundary material. The mechanical, tribological, chemical, electrical and bio-compatible properties of UNCD make it ideal for use in a variety of demanding environments.[1] Applications for UNCD range from the nano to macro-scale in areas such as microelectromechanical systems,[2,3] electronic power devices,[4] field-emission devices,[5] mechanical pumps,[6,7] biomedical devices[8,9] and biosensors.[10] As the demand for UNCD broadens, an understanding of its response to ionizing radiation and electron bombardment becomes critical. An understanding of these processes will pave the way to new, exciting opportunities and a range of applications in sensing, radiation shielding and MEMS technologies.

In this article, we report the structural modification of UNCD under extreme ionizing conditions which are simulated using electron irradiation in a scanning electron microscope (SEM). In situ Raman spectroscopy reveals decay of the Raman feature at $\sim$ 1140 cm^{-1} during electron exposure, which has previously been ascribed to hydrogen at grain boundaries.[11–13] The modified UNCD film is recovered on annealing to temperatures replicating material growth conditions[14] and the onset of hydrogen diffusion,[15] indicating that whilst hydrogen redistributes, it is not significantly desorbed from the material during electron exposure. Our results are consistent with and serve as evidence for the assignment of the $\sim$ 1140 cm^{-1} Raman peak to hydrogen, complement prior tentative interpretations of the effects of electron exposure on cathodoluminescence from polycrystalline diamond,[16] and implicate dehydrogenation of UNCD grain boundaries as the radiation-damage mechanism that is responsible for a loss of chemical inertness that gives rise to chemical etching of UNCD.[17]

Experimental Section

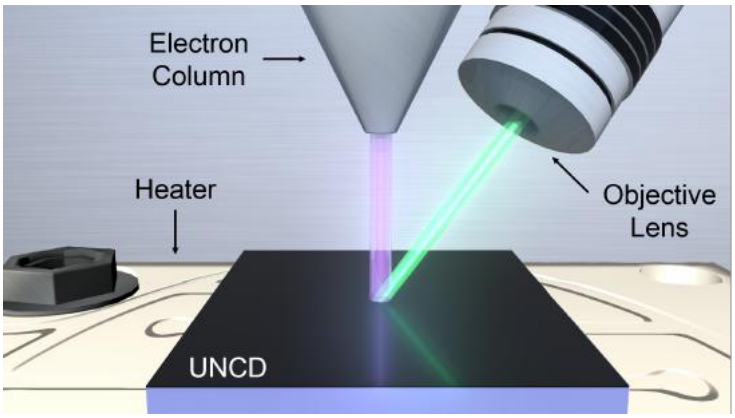

Figure 1: Rendering of the electron-laser beam system used to perform in situ heating and Raman spectroscopy. The electron column, objective lens of the Raman spectroscopy system, substrate heater and UNCD substrate are shown. The electron beam and laser are aligned to be coincident at the UNCD surface.

Electron irradiation experiments were performed under high vacuum ($\sim 3 \times 10^{-4}$ Pa) at various substrate temperatures using an FEI Company Quanta 3D FEG variable pressure[18] SEM equipped with a heating stage assembly (Figure 1). During irradiation, a 30 keV, 23 nA, focused electron beam was normal to the substrate surface and rastered across a 75 $\times$ 68 μm scan area discretized into 512 $\times$442 pixels with a dwell time of 10 μs per pixel. The substrate was a 1.7 μm film of UNCD grown on silicon (grain size = 2 - 5 nm, average roughness = 10 nm, UNCD Aqua 25 from Advanced Diamond Technologies, Inc.). Cleaning of the substrate was performed by first annealing in air at 500 K for $\sim$ 2 hours, followed by in situ plasma cleaning with oxygen radicals (primarily O_2^+ and O^+) at 575 K for $\sim$ 1 hour using an XEI Scientific Evactron[19] unit installed on the SEM (RF power = 13 W, O_2 pressure = 40 Pa).

In situ Raman spectroscopy measurements were performed using a custom system comprised of a 532 nm, 50 mW excitation laser ($<$ 0.001 nm spectrum width, FreeBeam 532 Raman Laser Module, RGBLase LLC), 10$\times$ objective (spot size: 3.3 - 6.7 μm Gaussian beam waist (w_0), 0.28 NA, Mitutoyo Plan Apo Infinity Corrected Long WD Objective) and QE65 Ocean Optics spectrometer unit. The laser angle of incidence was 60° and aligned to

be coincident with the electron irradiation area at the UNCD surface. Discrete-time spectra were collected over a Raman wavenumber shift range of 900 - 2100 cm^{-1} using a 10 s collection time for each frame.

Raman spectra were analyzed by fitting a third-order background and five Gaussian peak shape functions to the collected spectra using a routine written in the software package Mathematica.[20] Four of the peaks have previously been assigned to trans-polyactylene (TPA) at the grain boundary (ν_1 and ν_3) and carbon (D and G) components of the UNCD film.[11–13,21–26] A fifth peak (ν_2) has previously been assigned to TPA ($\sim$ 1210 cm^{-1}) or vibrational density of states contributions from small diamond grains ($\sim$ 1200 cm^{-1}), and is only observed via fitting.[25] The characteristic diamond Raman peak at 1332 cm^{-1} was not included in the analysis as its contribution is negligible in visible Raman analysis of films grown with minimal hydrogen in the plasma[13] and it was not discernible in any of the spectra. Constraints were applied to the peak fitting routine after an initial manual fit and based on previous studies[25,26] with the following tolerances: ν_1: 1136 - 1140 cm^{-1}, ν_2: 1205 - 1210 cm^{-1}, D: 1338 - 1342 cm^{-1}, ν_3: 1450 - 1455 cm^{-1}, and G: 1545 - 1550 cm^{-1}. Visualization of the change in background photoluminescence (PL) signal with electron irradiation was realized by fitting a first-order gradient to the third-order fitting over the range of 1050 - 1700 cm^{-1}.

Results and Discussion

First, we investigated structural changes in UNCD during electron irradiation at room temperature. A region of UCND film was irradiated with 30 keV electrons while collecting discrete-time Raman spectra (Figure 2a). Electron irradiation caused drastic changes in the Raman spectra with all features reducing in intensity. In particular, the intensity of the background PL signal and ν_1 are observed to decay significantly compared to the ν_2, D, ν_3 and G features. The background PL signal and ν_1 have previously been assigned to TPA at

the diamond grain boundary with ν_1 arising from the C-H bending mode. These previous assignments are consistent with our observations of material restructuring, as electron irradiation has a significant adverse impact on organic materials, particularly those which are heavily hydrogenated.[27] The difference between the rate of decay for the three TPA ascribed Raman features is surprising. This may be caused by the nature of the bonding configuration associated with each feature. The removal of hydrogen from a small portion of C-H bonds in the TPA chain may not necessarily lead to changes in the C-C bonding configuration of TPA. This could explain why we only see a change in the ν_1 Raman feature, and not ν_2 and ν_3. We note that electron beam induced heating is negligible given the large interaction volume and scan area of the electrons, and the bulk nature of the film.[27]

Electron exposure of UNCD in high vacuum is known to cause slow electron beam induced etching that is mediated by residual H_2O molecules.[28] To confirm that the changes in Raman spectra observed here are not caused by EBIE, the sample was irradiated overnight (57,470 s) using a 30 keV, 43 nA electron beam at a substrate temperature of 296 K. The region was imaged ex situ using the tapping mode of a Digital Instruments Dimension 3100 atomic force microscope (AFM), and analyzed using the software package Gwyddion[29] (Figure 2b). The material removal rate was determined to be 1.3 pm s^{-1} under these conditions. Removal of material by EBIE can therefore be eliminated as the cause of the dramatic decrease in Raman intensity immediately following electron exposure. We note that the observed changes do not recover if the electron beam is blanked for extended time periods during the exposure treatment, and they are not caused by the laser used for Raman spectroscopy (see the Supporting Information, sections S1 and S2). We also note that the observed changes in Raman spectra cannot be caused by carbonaceous films formed by electron beam induced deposition (EBID) of residual hydrocarbon contaminants. Such EBID competes with and is more efficient that H_2O-mediated EBIE (which also cause etching of the carbonaceous films).[30] Our observation of etching therefore serves as evidence for the fact that the buildup of carbonaceous films was negligible and outcompeted by EBIE.[31]

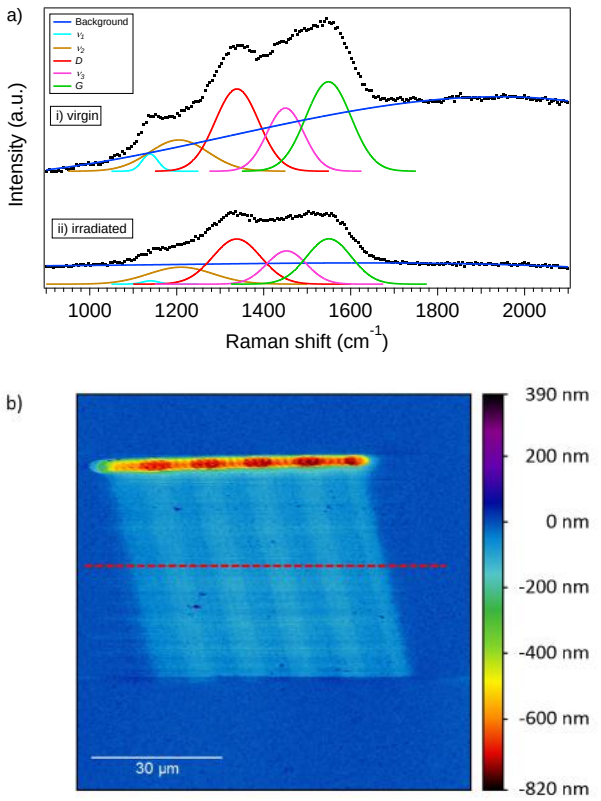

Figure 2: Electron beam induced restructuring of UNCD at room temperature. a) Raman spectra of (i) virgin UNCD and (ii) UNCD exposed to 30 keV electrons for $\sim$ 26 minutes. Also shown is the fitted PL background and Gaussian Raman peaks ν_1, ν_2, D, ν_3 and G. b) AFM image of an area of UNCD irradiated overnight by a 30 keV, 45 nA electron beam. (- - -) indicates the line scan position where the etch pit depth (75.6 nm) was determined. The yellow-orange region of the image is a deeper etch trench generated by an increase in the dwell-time of the electron beam at the edge of the scan box which is common in the rastered mode of a scanning electron microscope.

Next, we determined how UNCD temperature affects the dynamics of electron beam induced restructuring. Heating can provide insights into the mechanism of electron-induced restructuring with previous investigations reporting an increase in radiolysis associated restructuring with increasing temperature and knock-on displacement displaying little dependence on temperature.[27] Electron irradiations were performed on pristine regions of UNCD at a substrate temperature of 296, 588 and 684 K respectively (see Figure 3). At elevated temperatures the carbon D and G Raman peak intensities remain constant with electron exposure and the response of v_2 and v_3 relative to one another changes slightly. The PL back-

ground and v_1 however still show significant changes with electron exposure. To quantify the temperature dependence of electron-induced restructuring we determined the first-order rate constant (k) for the PL background and v_1 at 296, 588 and 684 K:

$$ln(n - n_{inf}) \;=\; -kt \;+\; ln(n_0 - n_{inf}) \tag{1}$$

where n is intensity at time (t), n_{inf} is the intensity at t = infinity, and n_0 is the intensity at $t = 0$. The rate constant of the electron-induced restructuring of the PL background is observed to increase slightly with temperature (k equals 0.0034, 0.0046 and 0.0060 s^{-1} at 296, 588 and 684 K respectively) (see the Supporting Information, section S3). We therefore ascribe the mechanism of restructuring to the background PL as radiolysis. The cause of this decrease in PL with electron irradiation is attributed to cleavage of nitrogen bonds within the nitrogen vacancy (NV) color center or deactivation of the NV color centers by formation of nonluminescent NVH_x centers enabled by the migration of hydrogen from the TPA chains in the grain boundary.[16] In comparison, the rate constant of the electron-induced restructuring of v_1 remains relatively constant and within the error of measurement (k equals 0.0018, 0.0028 and 0.0020 s^{-1} at 296, 588 and 684 K respectively). Given the large error in the measurement we cannot confirm if the nature of restructuring is knock-on displacement or radiolysis, however both would be expected at electron energies greater than 2 keV for hydrogen bonded carbon.[32] Changes in the D, G, v_2 and v_3 Raman features with temperature are not as simple to ascribe. The temperature-dependence of the response of the carbon D and G features to electron irradiation may be caused by an electron-driven chemical reaction that involves residual dopants in the film such as oxygen or nitrogen, however the exact mechanism is uncertain.

Finally, we investigated the effects of high temperature annealing on sample regions that were previously restructured by electrons. Two areas were selected for the study, (i) the region irradiated for 34 minutes at a substrate temperature of 684 K (Figure 3a), and an extreme case (ii) where the region was irradiated for 702 minutes using an electron beam

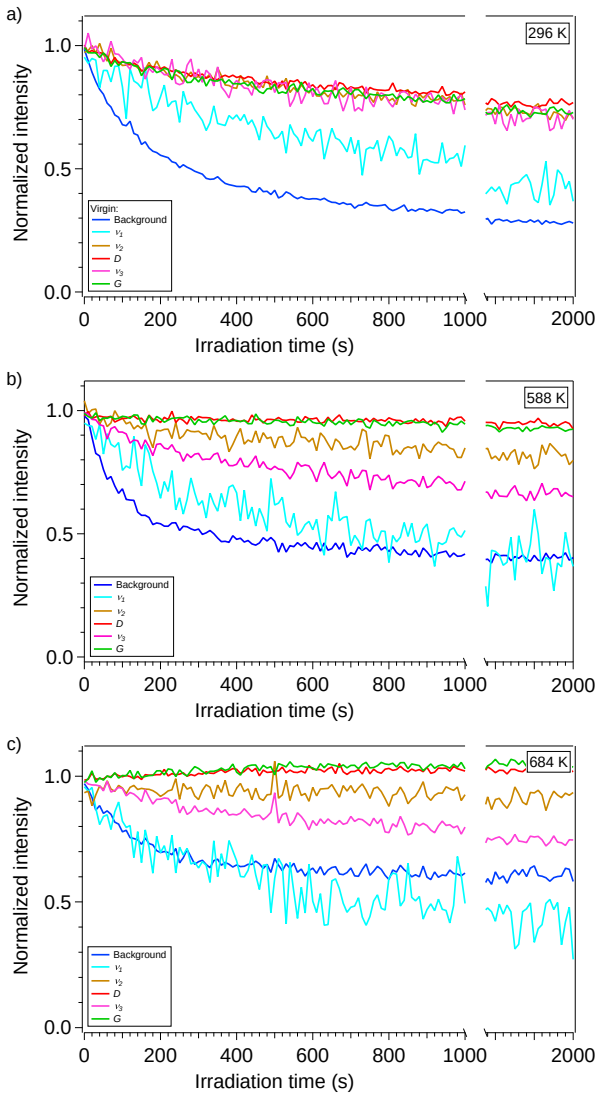

Figure 3: Electron beam induced restructuring of UNCD at substrate temperatures of 296, 588 and 684 K. (a-c) Normalized gradient of the background and intensity of ν_1, ν_2, D, ν_3 and G as a function of electron exposure time.

current of 45 nA at a substrate temperature of 588 K then irradiated for 26 minutes at a substrate temperature of 296 K. The sample was annealed at 883 K under high vacuum and then electron irradiation was performed on areas (i) and (ii), and a virgin region (Figure 4). We note that Raman measurements could not be performed at 883 K and the analysis was therefore done at room temperature.

Recovery of electron beam induced damage in UNCD was observed after in situ high-

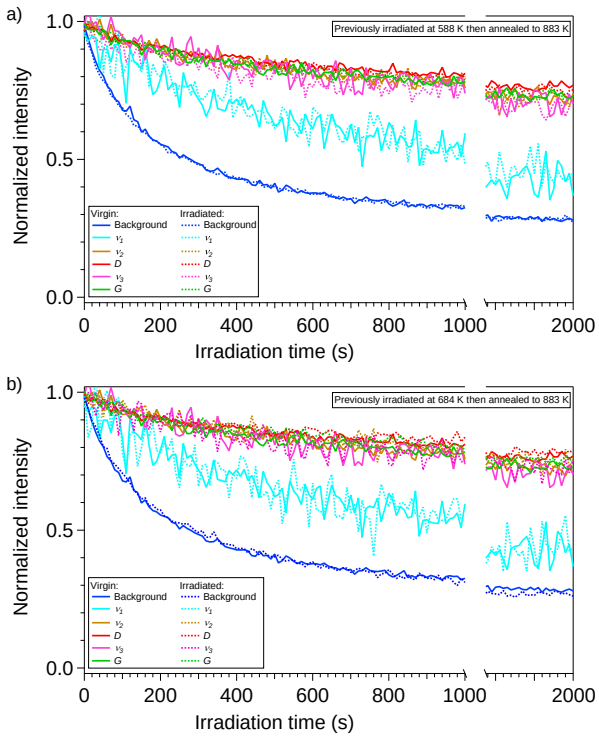

Figure 4: Recovery of electron beam induced damage in UNCD by high-temperature annealing. In situ annealing at 883 K under high-vacuum restores the Raman response of regions previously damaged by electrons to levels that are indistinguishable from virgin material. (a-b) After annealing, three UNCD regions were exposed to electron irradiation at room temperature: (a, dashed) a region previously irradiated with electrons at 588 K, area (i) (Figure 3a), (b, dashed) a region previously irradiated with electrons at 684 K, area (ii) (Figure 3b) and (a-b, solid) a virgin region.

temperature annealing. In fact, the sample regions that had been restructured by electrons are virtually indistinguishable from virgin UNCD after annealing in all aspects measurable by the Raman system: the normalized peak intensity and ratio, and intensity collected at the spectrometer (see the Supporting Information, section S4). Significantly the ratio of the hydrogen assigned ν_1 peak was restored after annealing. We ascribe the restoration of film quality to reconstruction of the electron modified TPA at the grain boundary of the nano-crystalline diamond. The annealing temperature (883 K) coincides with two critical temperatures: (1) the onset of the growth temperature for UNCD[14] and (2) diffusion of hydrogen within amorphous carbon material.[15] Therefore, recovery of the UNCD film by

thermal annealing shows that the film retains a large portion of displaced hydrogen.

Previous studies have revealed a temperature dependence of the preferred location of hydrogen within the structure of UNCD.[26] TPA chains are stable up to 1123 K, with temperatures greater than 1173 K resulting in the shortening of TPA chains and a subsequent decrease of the amount of hydrogen bonded to TPA chains in grain boundaries. During this transition however, the amount of hydrogen bonded to the surface of diamond grains increases. At 1273 K hydrogen is completely desorbed from the UNCD structure and the fraction of carbon in the diamond phase decreases. In the case of electron-induced damage presented here, it is proposed that during electron irradiation hydrogen is released from the TPA chains and migrates within the grain boundary. Subsequent thermal annealing at 883 K activates diffusion of hydrogen within the grain boundary and provides sufficient energy to overcome the barrier for recombination to a TPA chain, and therefore recovery of the damage.

Electron exposure has previously been observed to modify the chemical properties of UNCD. Specifically, pristine UNCD is highly inert and its chemical etch rate is negligible. However, the etch rate increases with electron beam exposure time during gas-mediated electron beam induced etching (EBIE) and this increase has been attributed to electron-induced radiation damage.[17] Based on the results presented here, the underlying mechanism can be attributed to a decrease in the concentration of hydrogenated diamond at grain boundaries. Dehydrogenation is known to lead to reconstruction of the structure,[33] and oxidation by H_2O molecules gives rise to electron-induced desorption of carbon species.[34]

Conclusions

In summary, in situ Raman spectroscopy measurements show that irradiation of UNCD with 30 keV electrons results in rapid structural changes to the film. The Raman peak assigned to hydrogen in grain boundaries decays significantly which we ascribe to efficient bond dissoci-

ation by the electron beam through desorption induced by electronic transitions or knock-on displacement processes. The temperature dependence of electron-induced damage to the background PL signal is revealed to differ from the Raman peak assigned to hydrogen in grain boundaries. The electron-induced damage mechanism of the background PL signal is ascribed to radiolysis based on this temperature dependence, which we ascribe to deactivation of NV color centers. Annealing of UNCD that was previously irradiated by electrons to 883 K under high-vacuum restores the structural properties of the film to those of pristine material. The annealing temperature corresponds to the onset of diffusion of hydrogen in amorphous carbon material and the growth temperature of UNCD. Our results have significant practical implications for the implementation of UNCD based devices and show in situ Raman spectroscopy to be a powerful tool for rapid material analysis.

Author Information

Corresponding Author

*E-mail: martin248@llnl.gov. Phone: +1 925 423 9218.

Author Contributions

Study conception and experiments were designed by A.A.M., and M.T. Experiments were conducted by J.F., M.S., S.R., A.B., and M.T. Data was analyzed and interpreted by A.A.M, and M.T. The paper was prepared by A.A.M., I.A., and M.T. All authors have given approval to the final version of the paper.

Notes

The authors declare no competing financial interest.

Acknowledgments

A portion of this work was performed under the auspices of the U.S. Department of Energy by Lawrence Livermore National Laboratory under Contract No. DE-AC52-07NA27344.

A portion of this work was funded by Thermo Fisher Scientific (formerly FEI Company) and the Australian Research Council (Project No. DP140102721). I.A. is the recipient of an Australian Research Council Discovery Early Career Research Award (Project No. DE130100592).

Associated Content

Supporting Information

S1: Pausing of electron irradiation during Raman spectroscopy; S2: Control experiment with no electron irradiation; S3: Integrated first-order reaction law fitting; S4: Recovery of electron-induced damage. This material is available free of charge via the Internet at http://pubs.acs.org/.

References

(1) Auciello, O.; Sumant, A. V. Status Review of the Science and Technology of Ultrananocrystalline Diamond (UNCD^{TM}) Films and Application to Multifunctional Devices. *Diamond Relat. Mater.* **2010**, *19*, 699–718.

(2) Krauss, A.; Auciello, O.; Gruen, D.; Jayatissa, A.; Sumant, A.; Tucek, J.; Mancini, D.; Moldovan, N.; Erdemir, A.; Ersoy, D.; Gardos, M.; Busmann, H.; Meyer, E.; Ding, M. Ultrananocrystalline Diamond Thin Films for MEMS and Moving Mechanical Assembly Devices. *Diamond Relat. Mater.* **2001**, *10*, 1952–1961.

(3) Adiga, V. P.; Sumant, A. V.; Suresh, S.; Gudeman, C.; Auciello, O.; Carlisle, J. A.; Carpick, R. W. Mechanical Stiffness and Dissipation in Ultrananocrystalline Diamond Microresonators. *Phys. Rev. B* **2009**, *79*, 245403.

(4) Alcantar-Peña, J.; Montes, J.; Arellano-Jimenez, M.; Aguilar, J. O.; Berman-Mendoza, D.; García, R.; Yacaman, M.; Auciello, O. Low Temperature Hot Filament

Chemical Vapor Deposition of Ultrananocrystalline Diamond Films with Tunable Sheet Resistance for Electronic Power Devices. *Diamond Relat. Mater.* **2016**, *69*, 207–213.

(5) Xiao, X.; Auciello, O.; Cui, H.; Lowndes, D.; Merkulov, V.; Carlisle, J. Synthesis and Field Emission Properties of Hybrid Structures of Ultrananocrystalline Diamond and Vertically Aligned Carbon Nanofibers. *Diamond Relat. Mater.* **2006**, *15*, 244–247.

(6) Sumant, A. V.; Krauss, A. R.; Gruen, D. M.; Auciello, O.; Erdemir, A.; Williams, M.; Artiles, A. F.; Adams, W. Ultrananocrystalline Diamond Film as a Wear-Resistant and Protective Coating for Mechanical Seal Applications. *Tribol. Trans.* **2005**, *48*, 24–31.

(7) Kovalchenko, A.; Elam, J.; Erdemir, A.; Carlisle, J.; Auciello, O.; Libera, J.; Pellin, M.; Gruen, D.; Hryn, J. Development of Ultrananocrystalline Diamond (UNCD) Coatings for Multipurpose Mechanical Pump Seals. *Wear* **2011**, *270*, 325–331.

(8) Shi, B.; Jin, Q.; Chen, L.; Auciello, O. Fundamentals of Ultrananocrystalline Diamond (UNCD) Thin Films as Biomaterials for Developmental Biology: Embryonic Fibroblasts Growth on the Surface of (UNCD) Films. *Diamond Relat. Mater.* **2009**, *18*, 596–600.

(9) Auciello, O.; Gurman, P.; Guglielmotti, M. B.; Olmedo, D. G.; Berra, A.; Saravia, M. J. Biocompatible Ultrananocrystalline Diamond Coatings for Implantable Medical Devices. *MRS Bull.* **2014**, *39*, 621–629.

(10) Yang, W.; Auciello, O.; Butler, J. E.; Cai, W.; Carlisle, J. A.; Gerbi, J. E.; Gruen, D. M.; Knickerbocker, T.; Lasseter, T. L.; Russell, J. N.; Smith, L. M.; Hamers, R. J. DNA-Modified Nanocrystalline Diamond Thin-Films as Stable, Biologically Active Substrates. *Nat. Mater.* **2002**, *1*, 253–257.

(11) Ferrari, A. C.; Robertson, J. Origin of the 1150 cm^{-1} Raman Mode in Nanocrystalline Diamond. *Phys. Rev. B* **2001**, *63*, 121405.

(12) Kuzmany, H.; Pfeiffer, R.; Salk, N.; Günther, B. The Mystery of the 1140 cm^{-1} Raman Line in Nanocrystalline Diamond Films. *Carbon* **2004**, *42*, 911–917.

(13) Birrell, J.; Gerbi, J.; Auciello, O.; Gibson, J.; Johnson, J.; Carlisle, J. Interpretation of the Raman Spectra of Ultrananocrystalline Diamond. *Diamond Relat. Mater.* **2005**, *14*, 86–92.

(14) Xiao, X.; Birrell, J.; Gerbi, J. E.; Auciello, O.; Carlisle, J. A. Low Temperature Growth of Ultrananocrystalline Diamond. *J. Appl. Phys.* **2004**, *96*, 2232.

(15) Kröger, H.; Ronning, C.; Hofsäss, H.; Neumaier, P.; Bergmaier, A.; Görgens, L.; Dollinger, G. Diffusion in Diamond-Like Carbon. *Diamond Relat. Mater.* **2003**, *12*, 2042–2050.

(16) Zachreson, C.; Martin, A. A.; Aharonovich, I.; Toth, M. Electron Beam Controlled Restructuring of Luminescence Centers in Polycrystalline Diamond. *ACS Appl. Mater. Interfaces* **2014**, *6*, 10367–10372.

(17) Martin, A. A.; Phillips, M. R.; Toth, M. Dynamic Surface Site Activation: A Rate Limiting Process in Electron Beam Induced Etching. *ACS Appl. Mater. Interfaces* **2013**, *5*, 8002–8007.

(18) Danilatos, G. Foundations of Environmental Scanning Electron Microscopy. *Adv. Electron. Electron Phys.* **1988**, *71*, 109–250.

(19) Isabell, T. C.; Fischione, P. E.; O'Keefe, C.; Guruz, M. U.; Dravid, V. P. Plasma Cleaning and Its Applications for Electron Microscopy. *Microscopy and Microanalysis* **1999**, *5*, 126–135.

(20) Wolfram Research, I. *Mathematica*, 10th ed.; Wolfram Research, Inc.: Champaign, Illinois, 2016.

(21) López-Ríos, T.; Sandré, É.; Leclercq, S.; Sauvain, É. Polyacetylene in Diamond Films Evidenced by Surface Enhanced Raman Scattering. *Phys. Rev. Lett.* **1996**, *76*, 4935–4938.

(22) Ferrari, A. C.; Robertson, J. Interpretation of Raman Spectra of Disordered and Amorphous Carbon. *Phys. Rev. B* **2000**, *61*, 14095–14107.

(23) Pfeiffer, R.; Kuzmany, H.; Knoll, P.; Bokova, S.; Salk, N.; Günther, B. Evidence for Trans-Polyacetylene in Nano-Crystalline Diamond Films. *Diamond Relat. Mater.* **2003**, *12*, 268–271.

(24) Michaelson, S.; Hoffman, A. Hydrogen Bonding, Content and Thermal Stability in Nano-Diamond Films. *Diamond Relat. Mater.* **2006**, *15*, 486–497.

(25) Klauser, F.; Steinmüller-Nethl, D.; Kaindl, R.; Bertel, E.; Memmel, N. Raman Studies of Nano- and Ultra-nanocrystalline Diamond Films Grown by Hot-Filament CVD. *Chem. Vap. Deposition* **2010**, *16*, 127–135.

(26) Hu, X. J.; Chen, X. H.; Ye, J. S. The Roles of Hydrogen in the Diamond/Amorphous Carbon Phase Transitions of Oxygen Ion Implanted Ultrananocrystalline Diamond Films at Different Annealing Temperatures. *AIP Adv.* **2012**, *2*, 042109.

(27) Egerton, R. F.; Li, P.; Malac, M. Radiation Damage in the TEM and SEM. *Micron* **2004**, *35*, 399–409.

(28) Martin, A. A.; McCredie, G.; Toth, M. Electron Beam Induced Etching of Carbon. *Appl. Phys. Lett.* **2015**, *107*, 041603.

(29) Nečas, D.; Klapetek, P. Gwyddion: An Open-Source Software for SPM Data Analysis. *Open Phys.* **2012**, *10*, 181–188.

(30) Toth, M.; Lobo, C. J.; Hartigan, G.; Ralph Knowles, W. Electron Flux Controlled

Switching Between Electron Beam Induced Etching and Deposition. *J. Appl. Phys.* **2007**, *101*, 054309.

(31) Toth, M.; Lobo, C. J.; Lysaght, M. J.; Vladár, A. E.; Postek, M. T. Contamination-Free Imaging by Electron Induced Carbon Volatilization in Environmental Scanning Electron Microscopy. *J. Appl. Phys.* **2009**, *106*, 034306.

(32) Egerton, R. Mechanisms of Radiation Damage in Beam-Sensitive Specimens, for TEM Accelerating Voltages Between 10 and 300 kV. *Microsc. Res. Tech.* **2012**, *75*, 1550–1556.

(33) Klauser, R.; Chen, J.-M.; Chuang, T.; Chen, L.; Shih, M.; Lin, J.-C. The Interaction of Oxygen and Hydrogen on a Diamond C(111) Surface: A Synchrotron Radiation Photoemission, LEED and AES Study. *Surf. Sci.* **1996**, *356*, L410–L416.

(34) Martin, A. A.; Bahm, A.; Bishop, J.; Aharonovich, I.; Toth, M. Dynamic Pattern Formation in Electron-Beam-Induced Etching. *Phys. Rev. Lett.* **2015**, *115*, 255501.

Graphical TOC Entry